Autonomous Flight Test of a Novel Non-conventional Biplane Micro Air Vehicle

Shuvrangshu Jana[1], Shashank Shivkumar[2], Mayur Shewale[3], Harikumar Kandath[4], Meghana Ramesh[5], Susheel Balasubramaniam[6], Eshaan Khanapuri[7], and M.Seetharama Bhat[8]

[1]Research Associate, Micro Air Vehicle Laboratory, Department of Aerospace Engineering, Indian Institute of Science, Bengaluru, India, Email: shuvra.ce@gmail.com

[2]Research Assistant, Micro Air Vehicle Laboratory, Department of Aerospace Engineering, Indian Institute of Science, Bengaluru, India, Email: shashank.shivkumar@gmail.com

[3]Research Assistant, Micro Air Vehicle Laboratory, Department of Aerospace Engineering, Indian Institute of Science, Bengaluru, India, Email: mayur.27391@gmail.com

[4]Research Associate, Micro Air Vehicle Laboratory, Department of Aerospace Engineering, Indian Institute of Science, Bengaluru, India, Email: harikumar100@gmail.com

[5]Research Associate, Micro Air Vehicle Laboratory, Department of Aerospace Engineering, Indian Institute of Science, Bengaluru, India, Email: meghanaramesh023@gmail.com

[6]Research Assistant, Micro Air Vehicle Laboratory, Department of Aerospace Engineering, Indian Institute of Science, Bengaluru, India, Email: susheels88@gmail.com

[7]Research Assistant, Micro Air Vehicle Laboratory, Department of Aerospace Engineering, Indian Institute of Science, Bengaluru, India, Email: ekhanapuri@yahoo.com

[8]Professor, Micro Air Vehicle Laboratory, Department of Aerospace Engineering, Indian Institute of Science, Bengaluru, India, Email: msbdcl19@gmail.com

ABSTRACT

This paper presents detailed mathematical modeling, controller design, and flight test results for the autonomous mission of a non-conventional fixed wing biplane Micro Air Vehicle (MAV) called

“Skylark" having span and chord length within 150 mm. Although numerous fixed wing MAV designs are reported in the open literature, a MAV’s reliable autonomous flight is still a challenge. The primary difficulties in performing the autonomous mission of fixed wing MAV are system integration within the weight and power budget, CG management, and flight controller design for fast dynamics. In this paper, the key challenges are addressed by using the higher payload capacity of “Skylark", suitable selection and design of avionics components, and design of controller after detailed development of the mathematical model, including the additional effect of propeller wash and motor counter torque. Autonomous flight test is successfully demonstrated after the validation of algorithms and software architecture through nonlinear six-dof simulation. The detailed design and development approach will increase MAV’s performance and reliability in civil and military applications.

INTRODUCTION

MAVs’ importance for difficult and dangerous tasks in civilian and military applications is increasing day by day. The era of MAVs officially began following the launch of the “Micro Air Vehicle" program by DARPA in 1997. Unmanned air vehicle whose maximum dimension is less than 150 mm and velocity around 10-20 m/s is generally classified as MAV (McMichael and Francis 1997). Fixed wing MAV outperforms other MAVs when the mission requirement involves high speed, long endurance, and high payload carrying capacity. Design and development issues related to fixed wing Micro Air vehicle is reported in various literature (Mueller et al. 2000; Wood et al. 2007; Michelson 2010; Moschetta 2014; Pipenberg and Maughmer 2015; Cai et al. 2014; Phan and Park 2020; Hassanalian and Abdelkefi 2017); however, outdoor flight tests results are reported in few cases such as SPOT (Hwang et al. 2002), Black Widow (Grasmeyer and Keennon 2001), Microbeacon (Suraj et al. 2013), KH2013A (Kandath et al. 2018). They are designed with capabilities of remote-controlled flight or stabilized flight. Black Widow is capable of altitude hold, airspeed hold, heading hold; KH2013A is capable of stabilized flight. Autonomous flight tests of fixed wing small UAVs having size more than 150 mm is reported in literature; for example, with 12 inch MAV (Platanitis and Shkarayev 2005), 27 cm MAV (Aboelezz et al. 2020), 30 cm MAV

(Albertani et al. 2005), 49 cm wingspan (Mohamed et al. 2016), (Zhao et al. 2015). However, a MAV having capabilities of autonomous navigation in an outdoor environment is not reported in the open literature.

Progress on research and development of MAV of size 150 mm slowed down due to difficulty in CG management of MAV with heavier payload and large avionics packages. The major issues involved in performing autonomous flight tests are system integration within weight and power budget, flight control design to handle the vehicle's fast dynamics (Michelson 2010). Different controller structure is proposed for small-scale UAVs platforms using model predictive controller (Campbell and Maciejowski 2009), switching PID controller (Zhu et al. 2007), dynamic inversion based neural network (He and Wu 2008), μ-synthesis (Fujinaga et al. 2007), linear quadratic gaussian controller (Lee et al. 2011). In case of MAVs, the controller design is reported using robust output feedback (Harikumar et al. 2019), PID controller (Aboelezz et al. 2021). Important challenges in developing a control algorithm for MAVs is due to the lack of high fidelity aerodynamic models in the presence of propeller flow and motor counter-torque (Harikumar et al. 2016). The detailed mathematical model also has to include effects of the propeller flow and motor-counter torque as these have significant effects on the overall forces and moments acting on MAV.

In this paper, the autonomous flight of MAV is made possible through efficient hardware design and software development after detailed mathematical modeling and analysis. In (Jana 2018), the design of a non- conventional biplane MAV called "Skylark" to have better payload capacity and higher static margin than the conventional MAVs is discussed. In this paper, the overall system configuration of "Skylark" is finalized, and flight test results of an autonomous mission are presented after detailed development of mathematical model and controller algorithm.

The autonomous navigation of "Skylark" is performed in the following stages. After the finalization of aerodynamic configuration, the avionics components are selected such that it satisfies the constraints of weight budget, power budget, and space budget. Then avionics components are distributed inside the vehicle in such a way that it helps in obtaining favorable CG location and balancing the counter-torque of the motor. Once every aspect of the vehicle configuration is decided, a mathematical model of the plant is developed using the CAD modeling, wind tunnel test, and standard empirical formula. As the contribution of propeller flow and motor counter-torque varies mostly with the motor RPM, the aerodynamic forces acting on the “Skylark" due to these parameters are modeled as a function of throttle RPM. The algorithms are designed after a detailed analysis of the mathematical model and validated through six-dof simulation. Initially, the stabilized flight is performed, where the control loop is handled through autopilot and guidance commands are generated from a pilot. The feedback from the stabilized flight test observations is considered for the adjustment of different system parameters. Finally, autonomous flight test is performed after analysis of various stabilized flight test data.

The rest of the paper is described as follows: Detailed of the system design of “Skylark" MAV for the autonomous mission is described in Section 2. In Section 3, the mathematical model of MAV is developed, and analysis for algorithm design is performed. Controller and estimation design is presented in Section 4. Six-dof simulation of MAV is discussed in Section 5. Autonomous flight test results are presented in Section 6.

SYSTEM DESIGN

“Skylark" is a non-conventional biplane MAV designed to carry the payload for the vision assisted autonomous navigation (Jana 2018; Jana et al. 2022). The important characteristics of “Skylark" are that it has an optimum top wing, which helps in achieving higher payload capacity as well as better stability margin. The span of the top and the bottom wing is kept the same; however, the chord length of the top wing is designed as 60 % of the chord length of the bottom wing considering the trade-off between payload carrying capacity and static longitudinal stability. This unconventional design improves the lift co-efficient of the vehicle while shifting the overall neutral point towards the trailing edge. “Skylark" has a higher range of allowable CG locations beyond the center of pressure location of the bottom wing due to its non-conventional biplane configuration. Passive techniques like asymmetric mass distribution about the forward axis and vertical tail placement in propeller wash are used to help balance counter torque. Aerofoils selected are of almost zero pitching moment and of high lift-coefficient. Control surfaces are designed considering handling quality as per “MIL-F8785C". In the Fig. 1, the fabricated model of the MAV “Skylark” is shown. The important aerodynamic parameters of the “Skylark” are shown in Table 1.

The aerodynamics responses of the MAV class of vehicles are highly sensitive to the motor-propeller combination. The basic aerodynamic configuration of a MAV is arrived at considering dummy payload and specific motor-propeller configuration. After the finalization of the aerodynamic configuration, the avionics components are selected, considering the following points.

- Overall system should be equipped with the sensors and computational units such that it can perform an autonomous mission.
- The weight of the components and the overall current consumption should be within the weight and power budget.
- The components' size and shape should be selected in an optimal manner such that components can be placed within the allowable CG location without violating the requirement of longitudinal stability.
- The components should be selected, such that the distribution of components will help in balancing the motor counter-torque passively.

The components are selected iteratively while checking the above conditions. The important components are the main controller unit, sensors, power module, telemetry module, GPS, electronic speed controller (ESC), two nos. of battery, camera module, etc. The main sensors include Altimeter, and 9-axis IMU consists of a gyroscope, accelerometer, magnetometer. Two batteries are used to provide separate power to the motor and main controller unit. The main control unit is designed based on a microprocessor so that the main autopilot tasks and the image processing tasks can be performed simultaneously on a single board. The single board was necessary to satisfy the constraints of weight, space, and CG location. The main controller unit, sensors, power module, telemetry module, GPS, and other interfaces are combined in an autopilot board of 35 mm $\times$ 65 mm and weight of 16 grams. The weight of the structure, motor-propeller, 2S battery, 1S battery, ESC, control servos, and camera module used are approximately 40 grams, 7 grams, 16 grams, 3 grams, 2 grams, 4 grams, and 5 grams respectively. The Airspeed sensor is not used in this case as the output of this sensor fitted to MAV is found to be inaccurate. This is due to the fact that MAVs are susceptible to gust as wind speed is comparable to MAV's velocity. Details of the avionics hardware are given in Table 2. Figure 2 shows the details of avionics inside MAV.

The components are placed to obtain a favorable CG location, and the mass distribution is made asymmetric to balance the counter-torque of the motor. Although torque balance can not be maintained at different airspeeds, the asymmetric mass distribution will always help balance the propeller torque throughout the speed regime". The components are placed as shown in Figure 3. In this case, the propeller rotates in a clockwise motion (from the rear side), and in turn, due to Newton's third law, the reaction force causing the MAV to rotate in an anticlockwise direction (roll towards left). So, the right side of the MAV x-axis is made relatively heavier compared to another side to balance the counter-torque passively. As shown in Fig. 2, the heavier 2S battery is placed on the right side. The exact location of the components is decided after observations from the initial flight tests. The autopilot is placed on the vibration dampening pad to reduce motor vibration's effect on accelerometer output.

After finalizing the overall configuration, mathematical model, algorithms are developed for autonomous missions and validated through simulations. A tentative flowchart for performing autonomous navigation is shown in Fig. 4. The feedback connection implies that algorithm design is performed iteratively after getting feedback from the simulations, stabilized flight, and autonomous flights.

PLANT MODELING AND ANALYSIS

The system modeling aims to develop a mathematical model to capture the system dynamics and describe the effects of the external forces on the system. Generally, for developing the mathematical model of small-scale vehicles, first principle modeling, system identification, and hybrid identification methods are used (Cai et al. 2014; Bogdanowicz et al. 2015). In first-principles modeling, the system parameters are obtained based on the basic aircraft mechanics, XFLR analysis, CAD modeling, wind tunnel test, and standard empirical results (Platanitis and Shkarayev 2005; Harikumar et al. 2016; Phang et al. 2014; Wu et al. 2018); whereas, in system identification methods, system parameters are estimated from the analysis of flight test results (Kumar et al. 2013; Armanini et al. 2015; Burri et al. 2018). In the hybrid model, preliminary results of first principle methods are further improved using the flight data (Armanini et al. 2016; Saderla et al. 2017). System identification methods are suitable for the development of a linearized model about the particular operating point; whereas, the first-principles approach or hybrid approach is preferred for the development of the complete nonlinear model. Complete nonlinear modeling of the UAVs is reported in the literature such as “Zaggi flying wing", “Aerosonde" (Beard and McLain 2009) etc. In the case of MAVs, aerodynamic parameters are estimated for 15 cm wingspan MAV from wind tunnel test and empirical formula without incorporating the propeller flow (Kuo et al. 2007). The contribution of propeller flow towards the system’s total lift and drag forces is reported in (Harikumar et al. 2016; Null et al. 2005; Spoerry and Wong 2001). In this section, kinematics and dynamics equations of the “Skylark” MAV is developed from the first principles approach.

MAV structure and its different components are modeled, and the moment of inertia for different axis and planes is calculated using SOLIDWORKS software. The value of the moment of inertia in xy plane and yz plane is not negligible due to the presence of top wing and asymmetric mass distribution. The moment of inertia of the “Skylark” is calculated from the SOLIDWORKS software and presented in Table 3, where J_{xx}, J_{yy}, J_{zz} are the moment of inertia of the MAV in x, y, z axis and J_{xy}, J_{xz}, J_{yz} are the moment of inertia in xy, xz and yz plane respectively.

The fundamental kinematics and dynamics equations are available in the various literature (Beard and McLain 2009). In this paper, the kinematics and dynamics equations are developed along the similar lines. The following standard state variables are used in the modelling of MAV: Position variables (p_n, p_e, p_d), component of inertial linear velocities along body frame (u, v, w), attitudes (ϕ, θ, ψ) and angular rates (p, q, r).

The kinematics motion of MAV are expressed in the following equations.

$$\begin{bmatrix} \dot{p}_n \\ \dot{p}_e \\ \dot{p}_d \end{bmatrix} = \begin{bmatrix} \mathrm{c}\theta\mathrm{c}\psi & \mathrm{s}\phi\mathrm{s}\theta\mathrm{c}\psi - \mathrm{c}\phi\mathrm{s}\psi & \mathrm{c}\phi\mathrm{s}\theta\mathrm{c}\psi + \mathrm{s}\phi\mathrm{s}\psi \\ \mathrm{c}\theta\mathrm{s}\psi & \mathrm{s}\phi\mathrm{s}\theta\mathrm{s}\psi + \mathrm{c}\phi\mathrm{c}\psi & \mathrm{c}\phi\mathrm{s}\theta\mathrm{s}\psi - \mathrm{s}\phi\mathrm{c}\psi \\ -\mathrm{s}\theta & -\mathrm{s}\phi\mathrm{c}\theta & \mathrm{c}\phi\mathrm{c}\theta \end{bmatrix} \begin{bmatrix} u \\ v \\ w \end{bmatrix} \tag{1}$$

where, c stands for cos and s stands for sin respectively in equation 1.

$$\begin{bmatrix} \dot{\phi} \\ \dot{\theta} \\ \dot{\psi} \end{bmatrix} = \begin{bmatrix} 1 & \sin\phi\tan\theta & \cos\phi\tan\theta \\ 0 & \cos\phi & -\sin\phi \\ 0 & \sin\phi\sec\theta & \cos\phi\sec\theta \end{bmatrix} \begin{bmatrix} p \\ q \\ r \end{bmatrix} \tag{2}$$

Let m is the mass of MAV, f_x, f_y, f_z are the component forces acting along the body frame x, y, and z axes respectively. Then, the forces and velocities expressed in the body frame of MAV as

$$m(\frac{dV_g^b}{dt_b} + \omega_{b/i}^b \times V_g^b) = f^b \tag{3}$$

where, $V_g^b = (u, v, w)^T$, $\quad \omega_{b/i}^b = (p, q, r)^T$, $\quad f^b = (f_x, f_y, f_z)^T$, $\times$ stands for cross product.

Equivalently,

$$\dot{u} = rv - qw + \frac{f_x}{m} \tag{4}$$

$$\dot{v} = pw - ru + \frac{f_y}{m} \tag{5}$$

$$\dot{w} = qu - pv + \frac{f_z}{m} \tag{6}$$

The total forces along the body axes are obtained by summing all the components of forces due to gravity $(f_{x_{\text{gravity}}}, f_{y_{\text{gravity}}}, f_{z_{\text{gravity}}})$, aerodynamics $(f_{x_{\text{aero}}}, f_{y_{\text{aero}}}, f_{z_{\text{aero}}})$ and propulsion $(f_{x_{\text{propulsion}}}, f_{y_{\text{propulsion}}}, f_{z_{\text{propulsion}}})$.

$$f_x = f_{x_{\text{gravity}}} + f_{x_{\text{aero}}} + f_{x_{\text{propulsion}}} \tag{7}$$

$$f_y = f_{y_{\text{gravity}}} + f_{y_{\text{aero}}} + f_{y_{\text{propulsion}}} \tag{8}$$

$$f_z = f_{z_{\text{gravity}}} + f_{z_{\text{aero}}} + f_{z_{\text{propulsion}}} \tag{9}$$

Similarly, angular momentum and angular velocities of MAV can be expressed in the body frame as

$$\frac{dh^b}{dt_b} + \omega^b_{b/i} \times h^b = m^b \tag{10}$$

where, $h^b = J\omega^b_{b/i}, m^b = (l, m, n)^T$; l, m, and n are moments acting on the body frame x, y, and z axes respectively and J is inertia matrix.

$$J = \begin{bmatrix} J_{xx} & -J_{xy} & -J_{xz} \\ -J_{xy} & J_{yy} & -J_{yz} \\ -J_{xz} & -J_{yz} & J_{zz} \end{bmatrix} \tag{11}$$

It is to be noted that in conventional fixed wing vehicles, J_{xy} and J_{yz} are considered as zero; however, in case of "Skylark" MAV, these values are not negligible due to the presence of top wing and asymmetric mass distribution.

The propulsive force is calculated based on the available dynamic thrust at a given RPM of the motor. Aerodynamic forces and moments are contributed due to free stream airflow as well as the flow due to the propeller. In the case of MAV, the propeller's contribution to the aerodynamic force is quite substantial (Sudhakar et al. 2017), and it should be included in the design. The effect of propeller flow on the dynamics is separately modeled considering the only flow of propeller with the variation of motor RPM in zero free stream velocity. The component of forces and moments due to propeller flow is modeled as a function of motor RPM (ω). The "Skylark" MAV has an elevon control surface, and its effect can be modeled as a combination of individual elevator and aileron control surface. The aerodynamic forces and moments will mainly depend on the the angle of attack (α), roll rate (p), pitch rate (q), yaw rate (r), elevator angle (δ_e), aileron angle (δ_a) and flow due to propeller motion.

$$f_{\text{Total}}(\alpha, p, q, r, \delta_e, \delta_a, \omega) = f_{\text{Free-stream}}(\alpha, p, q, r, \delta_e, \delta_a) + f_{\text{Propeller-flow}}(\omega) \tag{12}$$

$$m_{\text{Total}}(\alpha, p, q, r, \delta_e, \delta_a, \omega) = m_{\text{Free-stream}}(\alpha, p, q, r, \delta_e, \delta_a) + m_{\text{Propeller-flow}}(\omega) \tag{13}$$

Lift and drag forces are measured in the stability frame. The main parameters affecting the lift and drag forces are the angle of attack (α), pitch rate (q), elevator angle (δ_e), and flow due to propeller motion. Lift force is modeled along with the stability axis frame as follows:

$$F_{\text{Lift}} = \frac{1}{2}\rho V_a^2 S C_L(\alpha, q, \delta_e) + f_L(\omega) \tag{14}$$

$$F_{\text{Drag}} = \frac{1}{2}\rho V_a^2 S C_D(\alpha, q, \delta_e) + f_D(\omega) \tag{15}$$

where C_L and C_D are the lift coefficient and drag coefficient, $f_L(\omega)$ and $f_D(\omega)$ are the contribution of propeller flow towards the lift and drag forces, ρ is the density of air, V_a is the airspeed, and S is the reference area of the "Skylark" MAV. C_L and C_D are modeled with acceptable accuracy as

$$C_L = C_L(\alpha) + C_{L_q}\frac{c}{2V_a}q + C_L(\delta_e) \tag{16}$$

$$C_D = C_D(\alpha) + C_{D_q}\frac{c}{2V_a}q + C_D(\delta_e) \tag{17}$$

where, c is the chord of the bottom wing. The aerodynamic forces $f_{x_{\text{aero}}}$ and $f_{z_{\text{aero}}}$ are obtained after transforming F_{Lift} and F_{Drag} in body frame.

Similarly, the aerodynamic lateral force acting along y-axis depend on the sideslip angle (β), roll rate (p), yaw rate (r), aileron deflection (δ_a) and effect of propeller flow. The lateral force is modeled as follows:

$$f_{y_{\text{aero}}} = \frac{1}{2}\rho V_a^2 S C_Y(\beta, p, r, \delta_a) + f_Y(\omega) \tag{18}$$

$$C_Y = C_Y(\beta) + C_{Y_p}\frac{b}{2V_a}p + C_{Y_r}\frac{b}{2V_a}r + C_Y(\delta_a) \tag{19}$$

where, $f_Y(\omega)$ is the contribution of propeller flow towards lateral force, and b is the span of the bottom wing. The important factors which contribute to the rolling moment are sideslip angle (β), roll rate (p), yaw rate (r), aileron deflection (δ_a), flow due to propeller and motor counter-torque. So, the rolling moment is modeled as:

$$l = \frac{1}{2}\rho V_a^2 S b C_l\Big(\beta, p, r, \delta_a\Big) + f_l(\omega) \tag{20}$$

$$C_l = C_l(\beta) + C_{l_p}\frac{b}{2V_a}p + C_{l_r}\frac{b}{2V_a}r + C_l(\delta_a) \tag{21}$$

where $f_l(\omega)$ is the moment generated due to propeller flow and motor counter-torque. The moment generated from propeller flow is due to the creation of asymmetric flow around the propeller. In case of pitching moment, The angle of attack (α), pitch rate (q), elevator deflection (δ_e), and propeller flow are the main contributing factors. Therefore, pitching moment is modeled as:

$$m = \frac{1}{2}\rho V_a^2 S c C_m\Big(\alpha, q, \delta_e\Big) + f_m(\omega) \tag{22}$$

$$C_m = C_m(\alpha) + C_{m_q}\frac{c}{2V_a}q + C_m(\delta_e) \tag{23}$$

Similarly, the important variables behind the yawing moment are the same as the rolling moment, i.e., sideslip angle (β), roll rate (p), yaw rate (r), aileron angle (δ_a), and propeller flow. Yawing moment is modeled as

$$n = \frac{1}{2}\rho V_a^2 S b C_n\Big(\beta, p, r, \delta_a\Big) + f_n(\omega) \tag{24}$$

$$C_n = C_n(\beta) + C_{n_p}\frac{b}{2V_a}p + C_{n_r}\frac{b}{2V_a}r + C_n(\delta_a) \tag{25}$$

The contribution of propeller flow towards various forces and moments are listed in Table 4. The different coefficients of the force and moment equations are obtained through the wind tunnel test and using empirical formulas (Roskam 1990). The estimation method for the different coefficients in force and moment equations are listed in Table 8. The wind tunnel test of “Skylark" is conducted in closed test sections in an open circuit wind tunnel at Micro Air Vehicle Aerodynamic Research Tunnel (MART) in National Aerospace Laboratory (NAL) complex (Jana et al. 2020). The important wind tunnel characteristics are given in Table 5. The snapshot of the MAV placed in the wind tunnel is shown in Figure 5. The wind tunnel test is performed at the velocity range of 6-16 m/s and at different position of angle of attack ($0^o - 32^o$), angle of sideslip (-7^o to 7^o), motor RPM (9500-13500 RPM) and control surfaces. The static and control derivatives are listed in Table 6 and Table 7.

The plant’s non-linear model is linearized at the different operating points of the flight envelope for ease of controller design, and the static stability is checked at all points. The plant is linearised at different velocities ranging from 8-12 m/s and different flight conditions such as straight and level flight, climbing flight, turning flight. The non linear model of MAV, $\dot{x} = f(x, u)$ and $y = f(x)$ can be linearised about any operating point as:

$$\dot{x} = Ax + Bu; \quad y = Cx \tag{26}$$

where, x, u, y are the MAV states, control, and output variables; A, B, C are the system matrix, control input matrix, and output matrix.

The important states and control variables which affect the longitudinal dynamics are velocity in forward and downward direction, pitch rate, pitch angle, elevator and throttle input. In the case of straight and level flight at the velocity of 10 m/s, longitudinal dynamics for state variables $((x_{\text{long}}) = (u, w, q, \theta)^T$) and control variables$((u_{\text{long}}) = (\delta_e, \delta_t)^T)$ can be expressed as:

$$\dot{x}_{\text{long}} = A_{\text{long}} x_{\text{long}} + B_{\text{long}} u_{\text{long}}. \tag{27}$$

In this case,

$$A_{\text{long}} = \begin{pmatrix} -1.091 & 0.3773 & -1.832 & -9.641 \\ -0.6549 & -3.944 & 9.714 & -1.796 \\ 38.16 & -56.61 & -1.569 & 0 \\ 0 & 0 & 0.991 & 0 \end{pmatrix}$$

$$B_{\text{long}} = \begin{pmatrix} -0.3478 & 33.54 \\ 2.424 & -17.66 \\ -567.7 & -738.7 \\ 0 & 0 \end{pmatrix}$$

Similarly, lateral dynamics mainly depends on lateral velocity, roll rate, yaw rate and roll angle, and aileron input. The lateral dynamics can be expressed as for state ($x_{\text{lat}} = (v, p, r, \phi)^T$) and control ($u_{\text{lat}} = (\delta_a, \delta_t)^T$) is expressed as ;

$$\dot{x}_{\text{lat}} = A_{\text{lat}} x_{\text{lat}} + B_{\text{lat}} u_{\text{lat}}. \tag{28}$$

In this case,

$$A_{\text{lat}} = \begin{pmatrix} -0.8921 & 1.855 & -9.834 & 9.554 \\ -32.38 & -0.1321 & 0.1738 & 0 \\ 11.91 & -0.0335 & -3.326 & 0 \\ 0 & 1.0 & 0.1862 & 0 \end{pmatrix}$$

$$B_{\text{lat}} = \begin{pmatrix} 1.764 & 2.102 \\ 132.0 & -116.7 \\ 109.2 & -58.29 \\ 0 & 0 \end{pmatrix}$$

The different modes of the MAV are shown in Table 9. In the case of longitudinal dynamics, the complex pairs (-2.4476 +24.8028i and -2.4476 -24.8028i) are related to short period modes, and other pairs (-0.8544 + 1.4212i and -0.8544 - 1.4212i) are responsible for phugoid modes. Similarly, in the case of lateral dynamics, the complex pairs (-0.7032 +13.0454i and -0.7032 -13.0454i) are related to dutch-roll mode; however, in this case, the rolling mode and the spiral mode cannot be distinguished as typically done in larger UAVs.

Clearly, from Table 9, the longitudinal and lateral dynamics are statically stable for this operating point. Similarly, the static stability of different operating points at different flight conditions is checked and found to be stable. In the case of MAV, the coupled lateral and longitudinal model can be unstable, although the separate dynamics can be stable (Harikumar et al. 2016). In this case, the coupled dynamics for state ($x_{\text{coupled}} = (u, w, q, \theta, v, p, r, \phi)^T$) and control ($u_{\text{coupled}} = (\delta_e, \delta_a, \delta_t)^T$) is expressed as ,

$$\dot{x}_{\text{coupled}} = A_{\text{coupled}} x_{\text{coupled}} + B_{\text{coupled}} u_{\text{coupled}} \tag{29}$$

The system matrix A_{coupled} is given by:

$$A_{\text{coupled}} = \begin{pmatrix} -1.091 & 0.3773 & -1.832 & -9.641 & 0.0269 & 0 & -0.07 & 0 \\ -0.65 & -3.94 & 9.71 & -1.796 & 0.01 & 0.07 & 0 & 1.29 \\ 38.16 & -56.61 & -1.569 & 0 & -0.3467 & -0.002 & -0.0516 & 0 \\ 0 & 0 & 0.991 & 0 & 0 & 0 & 0.134 & -0.0197 \\ 0.20 & 0.038 & 0 & 0.2428 & -0.8921 & 1.855 & -9.834 & 9.554 \\ 4.07 & -0.1638 & -0.027 & 0 & -32.38 & -0.1321 & 0.1738 & 0 \\ 2.429 & -0.90 & -0.04 & 0 & 11.91 & -0.0335 & -3.326 & 0 \\ 0 & -0.02 & 0 & 0 & 0 & 1.0 & 0.1862 & 0 \end{pmatrix}$$

The different modes of this coupled dynamics are shown in Table 10. Comparing the eigenvalues of separate dynamics (from Table 9) with the coupled dynamics (from Table 10), it is observed that the eigenvalues are close to each other. It can be concluded that the effect of coupling is small for this MAV configuration; hence, the controller design for the longitudinal dynamics and the lateral dynamics can be performed separately.

ALGORITHM DESIGN

In this section, important algorithms required for an autonomous mission such as estimation, controller, and path planning algorithms are discussed. Accurate state estimation is of utmost importance for the system identification using the flight tests, guidance, and controller design of MAV. The overall mission is classified into different waypoints. The waypoint information is passed through the guidance block, and the desired height and course angle information are generated. For ease of implementation of guidance block, the guidance commands for the controller block can be generated using Lyapunov based vector field method (Nelson et al. 2007), (Lawrence et al. 2008), nonlinear guidance motivated from proportional navigation guidance algorithm (Park et al. 2004). In overall system architecture, the controller block must be designed very much specific to the vehicle dynamics. In an ideal case, the controller should be designed at different operating points, and gains are selected using gain scheduling techniques. The different operating points are mainly decided based on the airspeed, angle of attack, height. In this case, the airspeed and the angle of attack information are not available accurately; hence it is difficult to schedule the gains based on the operating points. So, the controller is designed considering the best representative plant. The controller is designed for a straight and level flight for the nominal velocity of 10 m/s. As discussed earlier, the coupling effects of longitudinal and lateral dynamics are not significant; hence, the controller for longitudinal dynamics and lateral dynamics is designed separately.

Controller Design

The controller block generates the control commands for the motor and control servos after considering the desired commands from the guidance loop and the MAV's present state from the estimation loop. Apart from ensuring overall system stability, controller design must be performed considering the handling qualities that determine the aircraft responses to external disturbances or pilot commands. In the MAV class of vehicles, no specification for the handling qualities requirement is available in the open literature. So, the specifications for controller design are considered from the MIL-F8785C with suitable adjustment for the MAV class of vehicles. The “Skylark" is classified as Class-IV and the controller design specifications are obtained considering flight operation in the category of phase C with a level of acceptability to be one. With this consideration, the controller design specifications from the handling point of view as per MIL-F8785C is shown in Table 11, ω_{n_s}, ω_{n_d}, ζ_s, ζ_{ph}, ζ_d are the short period frequency, dutch roll mode frequency, short period damping ratio, and phugoid mode damping ratio respectively (Sadraey 2012). Comparing the desired value and the present value of different parameters in Table 11, it is concluded that ζ_s and ζ_d, i.e., damping of the short period and the dutch roll mode needs to be improved.

The controller structure needs to be chosen to improve the damping of short period mode and dutch roll mode. The short period mode is motion in pitch plane involving pitch rate (q), pitch attitude (θ), and angle of attack (α). The dutch roll is an oscillation in the yaw plane, which combines roll and sideslip.

In the case of lateral dynamics, the transfer function from p(s) to $\delta_a(s)$:

$$\frac{p(s)}{\delta_a(s)} = \frac{131.9s^3 + 518.4s^2 + 50460s - 9090}{s^4 + 4.35s^3 + 180.7s^2 + 510.7s + 1004} \tag{30}$$

In the case of longitudinal dynamics, the transfer functions from q(s) to $\delta_e(s)$:

$$\frac{q(s)}{\delta_e(s)} = \frac{-566.7s^3 - 3009s^2 - 2764s - 2.159 \times 10^{-14}}{s^4 + 6.604s^3 + 632.3s^2 + 1075s + 1708} \tag{31}$$

After closed loop stability analysis, the pitch rate feedback is given to the elevator to improve the damping of short period mode. Similarly, roll rate feedback is given to the aileron to improve the damping of dutch roll mode. The lateral and the longitudinal controller block is driven by the desired course angle (χ_c) and the desired height (h_c) generated from the guidance block, respectively. The lateral and longitudinal controller block diagram details are shown in Figure 6 and Figure 7. In the block diagram, the value of the gain used in the controller structure is presented in Table 12. The closed-loop poles of the lateral and longitudinal dynamics are presented in Table 13.

Attitude Estimation

Angular rates (p,q,r) and positions (p_n, p_e, p_d) of MAV are available from the gyroscope and GPS respectively. So, in this case, accurate estimation of attitudes (ϕ, θ, ψ) form the available sensors is most important. Attitude estimation is performed using the Kalman filter framework where the attitude states are propagated using the data from gyroscopes, and the prediction is corrected using the information from the accelerometer and magnetometer. Accelerometer and magnetometer data is susceptible to noise due to vibration and the motor's magnetic flux with motor RPM variation. Multisensor fusion framework is used as data from the accelerometer and the magnetometer is not reliable at all operating points. Attitude estimation block diagram is shown in Fig. 8.

The sensor noises variance is calculated to form the sensor data log by conducting the remotely controlled flight tests. The accuracy of the estimation is checked using the motion simulator. In a motion simulator, the rate table is subjected to accurate angular rates, and its accurate angular position is recorded. The inner axis, middle axis, outer axis are subjected to roll, pitch, and yaw rates, respectively. The MAV is fitted with the motion simulator, and the estimation algorithm is verified by comparing the output of the estimator with the motion simulator's actual data. Also, the estimation output is checked after subjecting the vehicle to external vibrations. The estimation algorithm can be checked only with autopilot placement; however, the vehicle itself is put in the simulator just before flight tests to avoid the misalignment and orientation error involved with the placement of autopilot. A typical image during the estimation algorithm testing using motion simulator is shown in Fig. 9.

SIMULATION

The nonlinear MAV model of "SKYLARK" is simulated in MATLAB software. MAV needs to follow the waypoint path. As wind velocity is comparable to MAV velocity, MAVs are susceptible to gust. Total wind vector is considered as a combination of steady-state wind and a stochastic component consists of wind gust and atmospheric disturbances (Beard and McLain 2009). The stochastic gusts components are generated after passing the white noise through the Dryden transfer functions. The 3D coordinates of the waypoints to be followed are shown in Table 14. The guidance commands for the controller block is generated using the vector field method (Nelson et al. 2007).

The path followed by the MAV against the desired path is shown in Fig. 10. The tracking of desired course angle, roll angle, roll rate are shown in Fig. 11, Fig. 12, Fig. 13 respectively. The corresponding control command given to the aileron is shown in Fig.14. Similarly, in the case of longitudinal dynamics, Fig. 15, Fig. 16, Fig. 17, and Fig. 18 show the tracking of the desired height, pitch angle, roll rate and the corresponding control input respectively. Clearly, the plant is able to track the desired attitude and attitude rates during the waypoint mission. The control input to elevator (Fig. 18) and aileron (Fig. 14) is also bounded during the mission.

AUTONOMOUS FLIGHT TEST

In this section, details of the autonomous flight test of MAV is discussed. The tentative autopilot software architecture of "Skylark" MAV is shown in Fig. 19. The software architecture used in the autopilot is based on ardupilot firmware. The various sensor information is captured using the sensor acquisition block, and this information is used in the estimation block for state estimation. The estimation frequency is kept higher than the controller frequency. The guidance block generates the desired roll and pitch angle for the controller block. The controller block is operated at 50 Hz. The autopilot software is initially tested through Software in Loop Simulations (SILS) with virtual sensors and inside a virtual environment. The software is then further tested with Hardware in Loop Simulations (HILS) using the real autopilot hardware. HILS is performed with the help of a motion simulator.

Flight Testing

Once the SILS and HILS are performed successfully, the autonomous flight test is carried out in an outdoor environment. Since there are huge uncertainties involved with the manufacturing of MAV, few small duration remote-controlled (RC) flight tests are always performed to adjust the trim values of the control surface deflection before autonomous flights. MAV may undergo intermittent crash landing in this flight stage. After the successful initial RC tests of the vehicle, the system is further cross-checked for autonomous flight tests. The MAV is placed on flat ground, and the attitude angles are checked approximately. If there is an anomaly in the attitude angles, it is fixed after recalibration of the accelerometer and magnetometer as per the standard procedure.

MAV is launched with the hand in stabilized mode (Human Pilot is in the loop with autopilot) at an approximately fixed amount of jerk and at a fixed angle of attack. The allowable roll angle for the initial few seconds after launch is fixed to a particular angle. The MAV is subjected to autonomous mode (fully autonomous) once it gained a certain height and a certain velocity. During the take-off stage and landing, it is better to keep the pilot in the loop to counteract sudden gust as MAV is more susceptible to gust at these two critical stages. However, landing can be performed in autonomous mode. Flight test videos are included in this link [1].

Flight Test Results

"Skylark" has performed several successful flight tests in different weather conditions. One of the successful flight tests is described here. The results of one of several successful autonomous flight tests are described here. In this case, the take-off and landing are performed in a stabilized mode, and in between vehicle is flown in autonomous mode. The MAV is launched from the home location, and the consecutive waypoints are points 1, 2, and 3, respectively. If the MAV has reached within a radius of 30 m of a waypoint, it is considered that vehicle has reached the waypoint. The path of the vehicle using the logged GPS data during the waypoint mission is shown in Fig. 20. Clearly, the vehicle is able to perform the waypoint mission successfully, as it has reached within a radius of 30 m (drawn around the point). The 3D path of the vehicle using the GPS coordinates is

[1] Flight test videos

shown in Fig. 21. The MAV is launched at point A, and initially, it is in stabilized mode. At point B, the autonomous mode is switched on, and it performed the waypoint mission. After completing the waypoint mission, the MAV is put into stabilized mode again and landed successfully at point D.

The tracking response of the vehicle is analyzed from the recorded flight data. The commanded attitude angles and actual attitudes are plotted in Fig. 22, Fig. 24, Fig. 26; where the commanded portion is the duration where the vehicle was flying in autonomous mode. The commanded roll angle from the guidance loop and the achieved roll angle by MAV is shown in Fig. 22. The corresponding roll rate is plotted in Fig. 23. Similarly, the commanded pitch angle, achieved pitch angle, and the corresponding pitch rate is shown in Fig. 24 and Fig. 25. Likewise, for commanded yaw angle, achieved yaw angle, and the corresponding yaw rate is shown in Fig. 26 and Fig. 27.

It can be concluded that the tracking responses of the commanded roll and yaw angle are acceptable; however, tracking of pitch angle needs to be improved for improving the performance during the waypoint mission.

DISCUSSIONS

The crucial challenges of the autonomous mission of MAV are addressed through compact system design and efficient algorithm design. In the case of MAV, component placement plays a vital role in managing the CG location and balancing the counter torque. The designed MAV can handle wind speed up to 3 m/s. The tracking performance can vary based on the location of the waypoints and the direction of the wind. MAV can track the waypoints; however, the tracking performance in the longitudinal plane can be improved. Waypoints can be tracked with accuracy up to 20-30 m. The path between one point to another point may not be smooth due to uncertainty in system dynamics and the presence of wind gust. The performance can be improved by reducing the uncertainty in the system dynamics and plant modeling. Due to the complex dynamics involved with the MAV system, there may be uncertainty in MAV modeling. So, in some cases, some of the algorithm's parameters may need to be modified after observation of the flight tests as the developed plant model may not capture the real flight dynamics. It is not easy for a fixed gain based controller to handle the uncertainties involved in the complex MAV dynamics. An advanced controller, such as an adaptive controller, needs to be considered for the MAV controller design to adapt to uncertain MAV dynamics.

CONCLUSIONS

In this paper, autonomous navigation of a fixed-wing nonconventional biplane MAV “Skylark", having span and chord length within 150 mm, is presented. The main challenges of an autonomous mission for overall system integration, model development, and controller design are addressed. The key issues of overall vehicle configuration design, such as weight budget, power budget, CG management, balancing counter-torque, are addressed through proper selection, design, and strategical placement of avionics components. The significant effects of motor counter torque and propeller flow on the MAV dynamics are considered to develop a detailed mathematical model through wind tunnel tests. The controller is designed after a detailed analysis of the mathematical model and validated through six-dof simulation, SILS and HILS. Finally, the autonomous flight test is performed successfully through multiple waypoints. It is recommended that the uncertainties involved in the system dynamics need to be handled properly for better mission performance. The proposed design approach for autonomous navigation in this paper will improve the capabilities of the MAV class of vehicles.

DATA AVAILABILITY STATEMENT

Some or all data, models, or code that support the findings of this study are available from the corresponding author upon reasonable request.

ACKNOWLEDGMENTS

The authors would like to express their gratitude to Titas Bera and Sidhant Dhall for their suggestions to the MAV system design. The work is funded under National Program for Micro Air Vehicle (NP-MICAV) project of Defence Research Development Organization (DRDO). The authors would like to thank the Aeronautics Research and Development Board (ARDB) for their funding and support for the project.

REFERENCES

Aboelezz, A., Hassanalian, M., Desoki, A., Elhadidi, B., and El-Bayoumi, G. (2020). "Design, experimental investigation, and nonlinear flight dynamics with atmospheric disturbances of a fixed-wing micro air vehicle." *Aerospace Science and Technology*, 97, 105636.

Aboelezz, A., Mohamady, O., Hassanalian, M., and Elhadidi, B. (2021). "Nonlinear flight dynamics and control of a fixed-wing micro air vehicle: Numerical, system identification and experimental investigations." *Journal of Intelligent & Robotic Systems*, 101(3), 1–18.

Albertani, R., Boria, F., Bowman, S., Claxton, D., Ifju, P., Johnson, B., and Sytsma, M. (2005). "The university of florida autonomous micro air vehicle." *International Micro Air Vehicle Competition*.

Armanini, S. F., Caetano, J. V., de Visser, C. C., de Croon, G. C., and Mulder, M. (2016). "Aerodynamic model identification of a clap-and-fling flapping-wing mav: a comparison between quasi-steady and black-box approaches." *AIAA Atmospheric Flight Mechanics Conference*, 0014.

Armanini, S. F., de Visser, C. C., and de Croon, G. (2015). "Black-box lti modelling of flapping-wing micro aerial vehicle dynamics." *AIAA Atmospheric Flight Mechanics Conference*, 0234.

Beard, R. and McLain, T. (2009). "Navigation, guidance and control of small unmanned aircraft." *Princeton University Press, New Jersey*.

Bogdanowicz, C., Hrishikeshavan, V., and Chopra, I. (2015). "Development of a quad-rotor biplane mav with enhanced roll control authority in fixed wing mode." *American Helicopter Society, 71st Annual Forum*.

Burri, M., Bloesch, M., Taylor, Z., Siegwart, R., and Nieto, J. (2018). "A framework for maximum likelihood parameter identification applied on mavs." *Journal of Field Robotics*, 35(1), 5–22.

Cai, G., Dias, J., and Seneviratne, L. (2014). "A survey of small-scale unmanned aerial vehicles: Recent advances and future development trends." *Unmanned Systems*, 2(02), 175–199.

Campbell, C. and Maciejowski, J. (2009). "Control and guidance of a highly-flexible micro air vehicle using model predictive control." *Aiaa guidance, navigation, and control conference*, 5874.

Fujinaga, J., Tokutake, H., and Sunada, S. (2007). "Development of small unmanned aerial vehicle and flight controller design." *AIAA Atmospheric Flight Mechanics Conference and Exhibit*, 6501.

Grasmeyer, J. and Keennon, M. (2001). "Development of the black widow micro air vehicle." *39th aerospace sciences meeting and exhibit*, 127.

Harikumar, K., Dhall, S., and Bhat, M. S. (2016). "Nonlinear modeling and control of coupled dynamics of a fixed wing micro air vehicle." *Indian Control Conference (ICC), 2016*, IEEE, 318–323.

Harikumar, K., Dhall, S., and Bhat, S. (2019). "Design and experimental validation of a robust output feedback control for the coupled dynamics of a micro air vehicle." *International Journal of Control, Automation and Systems*, 17(1), 155–167.

Hassanalian, M. and Abdelkefi, A. (2017). "Classifications, applications, and design challenges of drones: A review." *Progress in Aerospace Sciences*, 91, 99–131.

He, G.-l. and Wu, G.-h. (2008). "Simulation of dynamic inversion with neural network and its applications to mav." *Intelligent Networks and Intelligent Systems, 2008. ICINIS'08. First International Conference on*, IEEE, 60–63.

Hwang, H., Chung, D., Yoon, K., Park, H., Lee, Y., and Kang, T. (2002). "Design and flight test of a fixed wing mav." *1st UAV Conference*, 3413.

Jana, S. (2018). "Novel biplane micro air vehicle system with adaptive control and vision augmentation." Ph.D. thesis, Indian Institute of Science, Bengaluru, India.

Jana, S., Kandath, H., Shewale, M., and Bhat, M. S. (2020). "Effect of propeller-induced flow on the performance of biplane micro air vehicle dynamics." *Proceedings of the Institution of Mechanical Engineers, Part G: Journal of Aerospace Engineering*, 234(3), 716–728.

Jana, S., Kandath, H., Shewale, M., Dhingra, G., Sai Harish, D., and Bhat, M. S. (2022). "Design and development of a novel fixed-wing biplane micro air vehicle with enhanced static stability." *CEAS Aeronautical Journal*.

Kandath, H., Pushpangathan, J. V., Bera, T., Dhall, S., and Bhat, M. S. (2018). "Modeling and closed loop flight testing of a fixed wing micro air vehicle." *Micromachines*, 9(3), 111.

Kumar, R., Ghosh, A., and Misra, A. (2013). "Parameter estimation from flight data of hansa-3 aircraft using quasi-steady stall modeling." *Journal of Aerospace Engineering*, 26(3), 544–554.

Kuo, Z.-S., Soong, C.-Y., and Chang, Y.-S. (2007). "Dynamic modeling and analysis of a whole-wing micro air vehicle." *48th AIAA/ASME/ASCE/AHS/ASC Structures, Structural Dynamics, and Materials Conference*, 2238.

Lawrence, D. A., Frew, E. W., and Pisano, W. J. (2008). "Lyapunov vector fields for autonomous unmanned aircraft flight control." *Journal of Guidance, Control, and Dynamics*, 31(5), 1220–1229.

Lee, C.-S., Chan, W.-L., Jan, S.-S., and Hsiao, F.-B. (2011). "A linear-quadratic-gaussian approach for automatic flight control of fixed-wing unmanned air vehicles." *The Aeronautical Journal*, 115(1163), 29–41.

McMichael, J. M. and Francis, M. S. (1997). "Micro air vehicles-toward a new dimension in flight." *DARPA document*.

Michelson, R. C. (2010). "Overview of micro air vehicle system design and integration issues." *Encyclopedia of Aerospace Engineering*.

Mohamed, A., Abdulrahim, M., Watkins, S., and Clothier, R. (2016). "Development and flight testing of a turbulence mitigation system for micro air vehicles." *Journal of Field Robotics*, 33(5), 639–660.

Moschetta, J.-M. (2014). "The aerodynamics of micro air vehicles: technical challenges and scientific issues." *International Journal of Engineering Systems Modelling and Simulation 48*, 6(3-4), 134–148.

Mueller, T. J., Shkarayev, S. V., and Ifju, P. (2000). *Introduction to the design of fixed-wing micro air vehicles*. American Institute of Aeronautics and Astronautics.

Nelson, D. R., Barber, D. B., McLain, T. W., and Beard, R. W. (2007). "Vector field path following for miniature air vehicles." *IEEE Transactions on Robotics*, 23(3), 519–529.

Null, W., Noscek, A., and Shkarayev, S. (2005). "Effects of propulsive-induced flow on the aerodynamics of micro air vehicles." *23rd AIAA Applied Aerodynamics Conference*, 4616.

Park, S., Deyst, J., and How, J. (2004). "A new nonlinear guidance logic for trajectory tracking."

AIAA guidance, navigation, and control conference and exhibit, 4900.

Phan, H. V. and Park, H. C. (2020). "Mimicking nature's flyers: a review of insect-inspired flying robots." *Current Opinion in Insect Science*.

Phang, S. K., Li, K., Yu, K. H., Chen, B. M., and Lee, T. H. (2014). "Systematic design and implementation of a micro unmanned quadrotor system." *Unmanned Systems*, 2(02), 121–141.

Pipenberg, B. T. and Maughmer, M. D. (2015). "Mission-driven design and fabrication of fixed-, flapping-, and rotary-wing micro air vehicles." *53rd AIAA Aerospace Sciences Meeting*, 0037.

Platanitis, G. and Shkarayev, S. (2005). "Integration of an autopilot for a micro air vehicle." *Infotech@ Aerospace*, 7066.

Roskam, J. (1990). *Airplane design, volume 6*. Roskam aviation and engineering corporation.

Saderla, S., Rajaram, D., and Ghosh, A. (2017). "Parameter estimation of unmanned flight vehicle using wind tunnel testing and real flight data." *Journal of Aerospace Engineering*, 30(1), 04016078.

Sadraey, M. H. (2012). *Aircraft design: A systems engineering approach*. John Wiley & Sons.

Spoerry, M. T. and Wong, K. (2001). "Design and development of a micro air vehicle (μav) concept: Project bidule." *The 9th Annual International Aerospace Congress. School of Aerospace, Mechanical and Mechatronic Engineering, University of Sydney, NSW, Australia*.

Sudhakar, S., Chandankumar, A., and Venkatakrishnan, L. (2017). "Influence of propeller slipstream on vortex flow field over a typical micro air vehicle." *The Aeronautical Journal*, 121(1235), 95–113.

Suraj, C., Sharma, H., Murari, V., Narayanan, P., and Ahmed, S. (2013). "Configuration design of 150 mm autonomous micro air vehicle–microbeacon.

Wood, R. J., Avadhanula, S., Steltz, E., Seeman, M., Entwistle, J., Bachrach, A., Barrows, G., and Sanders, S. (2007). "An autonomous palm-sized gliding micro air vehicle." *IEEE Robotics & Automation Magazine*, 14(2), 82–91.

Wu, L., Ke, Y., and Chen, B. M. (2018). "Systematic modeling of rotor-driving dynamics for small unmanned aerial vehicles." *Unmanned Systems*, 6(02), 81–93.

Zhao, L., Wang, D., Huang, B., and Xie, L. (2015). "Distributed filtering-based autonomous navigation system of uav." *Unmanned systems*, 3(01), 17–34.

Zhu, R., Sun, D., and Zhou, Z. (2007). "Integrated design of trajectory planning and control for micro air vehicles." *Mechatronics*, 17(4-5), 245–253.

List of Tables

TABLE 1. Important MAV parameters

Parameters	Value
Designed take-off mass	110 g
Nominal velocity	10 m/s
Top wing span	150 mm
Top wing chord	85 mm
Bottom wing span	150 mm
Bottom wing chord	140 mm
Vertical tail (area)	5600 mm^2
Vertical tail (height)	80 mm
Top wing airfoil	Modified MH-60
Bottom wing airfoil	Modified MH-60
Control surface	Elevon
Motor	AP05 5000 kv
Propeller	GWS 5030

TABLE 2. MAV avionics

Component	Description
Main controller unit	i.MX6 Freescale dualcore processor
Sensors	IMU (MPU-9250)
	Altimeter(MS5803-01BA)
	GPS (ORG-1411)
	camera
Telemetry	DRF4463F(433 MHz)
ESC	YEP-7A
Battery	2S: 300 mAh 35-70 C
	1S: 270 mAh 15 C
RAM	512 MB

TABLE 3. MAV moment of inertia

Axis	Value	
J_{xx}	3.3211×10^{-4}	kg − m^2
J_{yy}	2.7542×10^{-4}	kg − m^2
J_{zz}	3.0309×10^{-4}	kg − m^2
J_{xy}	0.0323×10^{-4}	kg − m^2
J_{xz}	0.7618×10^{-4}	kg − m^2
J_{yz}	0.0536×10^{-4}	kg − m^2

TABLE 4. Propeller contribution at zero free-stream velocity

Quantity	Value
$f_L(\omega)$	$0.0022 - 4.6\delta_\omega + 11\delta_\omega^2 - 5.8\delta_\omega^3$
$f_D(\omega)$	$-0.003466 + 15.86\delta_\omega - 52.19\delta_\omega^2 + 57.52\delta_\omega^3 - 21.01\delta_\omega^4$
$f_Y(\omega)$	$6.658 \times 10^{-7} - 0.4782\delta_\omega + 1.188\delta_\omega^2 - 0.639\delta_\omega^3$
$f_l(\omega)$	$0.00041 + 0.05326\delta_\omega - 0.1351\delta_\omega^2 + 0.06991\delta_\omega^3$
$f_m(\omega)$	$-0.00019 + 0.33\delta_\omega - 0.8229\delta_\omega^2 + 0.4173\delta_\omega^3$
$f_n(\omega)$	$-0.0000997 + 0.01316\delta_\omega - 0.03349\delta_\omega^2 + 0.01925\delta_\omega^3$

TABLE 5. Wind tunnel details

Specification	Value
Contraction ratio	9:1
Test section	0.8 m x 1.2 m x 2.5m
Velocity range	1-45 m/s
Mean flow velocity variation	+- 0.1 percent
Flow angularity	$< 0.1^0$
Free stream turbulent intensity	<0.18 percent
Range of angle of attack	$-5^0 - 32^0$
Range of sideslip angle	$-7^0 - +7^0$

TABLE 6. Static and control derivatives

Derivatives	Value at free-stream velocity of 8 m/s
$C_L(\alpha)$	$-0.065 + 2.9\alpha - 2\alpha^2$
$C_L(\delta_e)$	$0.92\ \delta_e$
$C_D(\alpha)$	$0.15 + 0.1\alpha + 1.5\alpha^2$
$C_D(\delta_e)$	$-0.06332\delta_e + 0.176\delta_e^2$
$C_Y(\beta)$	$0.05 - 0.58\beta$
$C_Y(\delta_a)$	$0.1148\delta_a$
$C_l(\beta)$	$-0.46\beta - 0.0059$
$C_l(\delta_a)$	$0.14\delta_a$
$C_m(\alpha)$	$0.24 - 0.73\alpha,$
$C_m(\delta_e)$	$-0.5617\delta_e + 0.5703\delta_e^2$
$C_n(\beta)$	$0.24\beta - 0.011$
$C_n(\delta_a)$	$0.09087\delta_a$

TABLE 7. Dynamic derivatives

Derivatives	Value
C_{L_q}	1.1339,
C_{D_q}	0
C_{Y_p}	0.0
C_{Y_r}	0.0
C_{l_p}	-0.0216
C_{l_r}	0.1639
$C_m(q)$	-0.2609
C_{n_p}	0.0
C_{n_r}	-0.5375

TABLE 8. Model parameter estimation

Quantity	Wind tunnel test	Empirical formula
Lift force	$C_L(\alpha), C_L(\delta_e), f_L(\omega)$	C_{L_q}
Drag force	$C_D(\alpha), C_D(\delta_e), f_D(\omega)$	C_{D_q}
Side force	$C_Y(\beta), C_Y(\delta_a), f_Y(\omega)$	C_{Y_p}, C_{Y_r}
Rolling moment	$C_l(\beta), C_l(\delta_a), f_l(\omega)$	C_{l_p}, C_{l_r}
Pitching moment	$C_m(\alpha), C_m(\delta_e), f_m(\omega)$	C_{m_q}
Yawing moment	$C_n(\beta), C_n(\delta_a), f_n(\omega)$	C_{n_p}, C_{n_r}

TABLE 9. Different modes of MAV

Longitudinal dynamics	Lateral dynamics
-2.4476 +24.8028i	-0.7032 +13.0454i
-2.4476 -24.8028i	-0.7032 -13.0454i
-0.8544 + 1.4212i	-1.4718 + 1.9285i
-0.8544 - 1.4212i	-1.4718 - 1.9285i

TABLE 10. Different modes of coupled dynamics of MAV

Coupled dynamics	Coupled dynamics
-2.4484 + 24.8023i	-0.70 + 13.0556i
-2.4484 -24.80323i	-0.70 - 13.0556i
-0.9266 + 1.3067i	-1.4020 +1.9750 i
-0.9266 + 1.3067i	-1.4020 -1.9750 i

TABLE 11. Handling qualities requirement as per MIL-F8785C

Parameters	Desired value	Present value
ω_{n_s}	0.4 (minimum)	24.92 rad/s
ω_{n_d}	1.0 (minimum)	13.064 rad/s
ζ_s	0.35-1.3	0.098
ζ_{ph}	0.04 (minimum)	0.515
ζ_d	0.08 (minimum)	0.05
$\zeta_d \omega_{n_d}$	1	0.65

TABLE 12. Different parameters of controller structure

Lateral dynamics		Longitudinal dynamics	
Gain variable	Value	Gain variable	Value
$k_{i\chi}$	2.56	k_{ih}	1.41
$k_{p\chi}$	2.86	k_{ph}	1.36
$k_{p\phi}$	0.021	$k_{i\theta}$	-0.001
$k_{p\phi}$	0.4	$k_{p\theta}$	-4.5
k_{ip}	-0.018	k_{pq}	-0.15
k_{pp}	0.002		

TABLE 13. Closed loop poles of MAV

Longitudinal dynamics	Lateral dynamics
-77.9484 +0.0i	-0.589 +13.21i
-12.2718 +0.0i	-0.589 -13.21i
-0.6944 + 1.1416i	-0.0238 + 0.525i
-0.6944 - 1.1416i	-0.0238 - 0.525i

TABLE 14. Waypoint path following

Points	Co-ordinates
Initial position	(0,0,0)
Point 1	(50,0,20)
Point 2	(400, 0, 20)
Point 3	(200,200, 20)
Point 4	(0,0, 10)

List of Figures

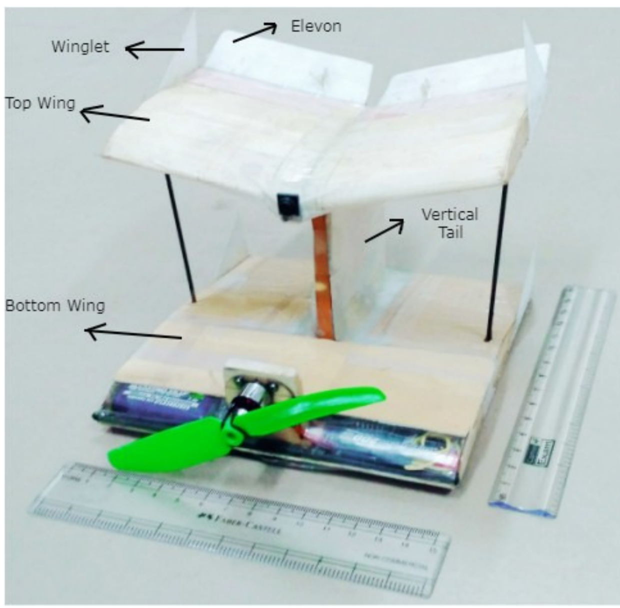

Fig. 1. “Skylark" MAV

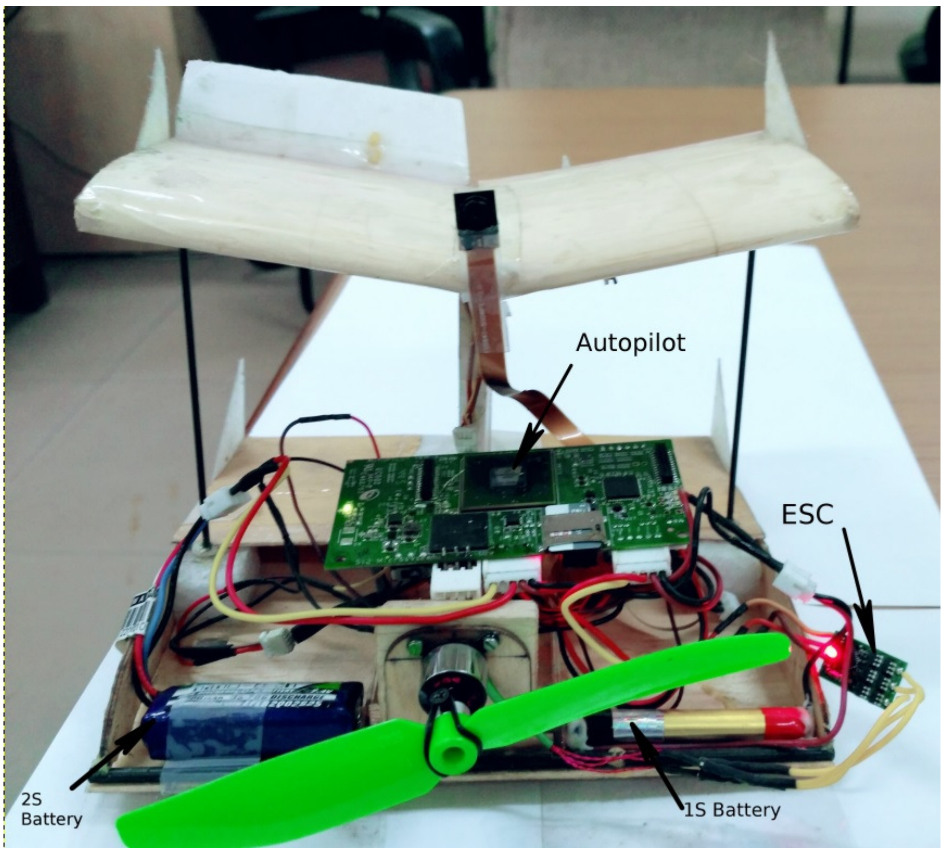

Fig. 2. MAV avionics

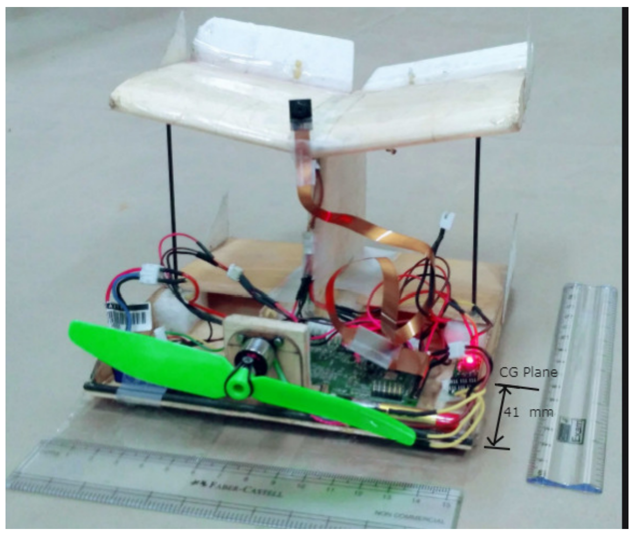

Fig. 3. Component placement

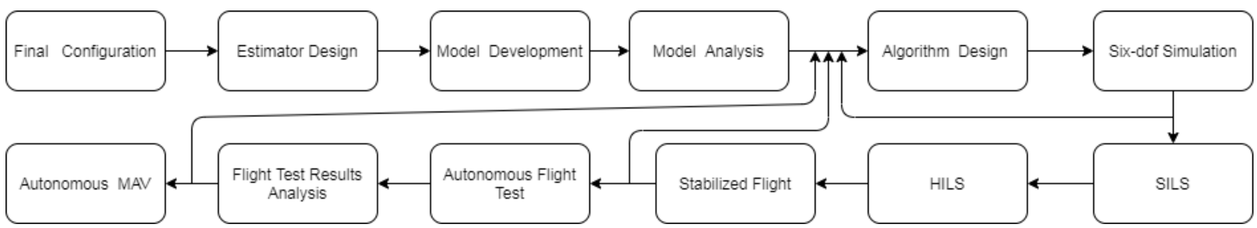

Fig. 4. Autonomous navigation flow chart

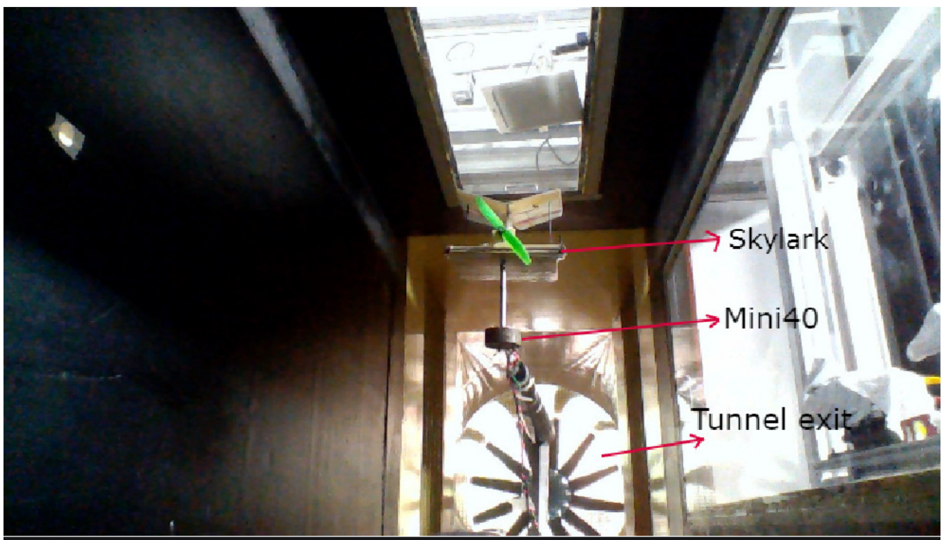

Fig. 5. Snapshot of MAV placed in windtunnel

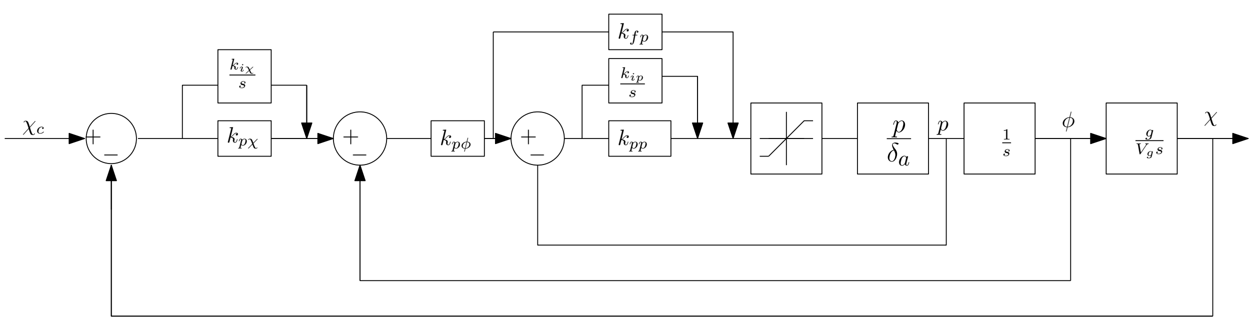

Fig. 6. Lateral controller structure

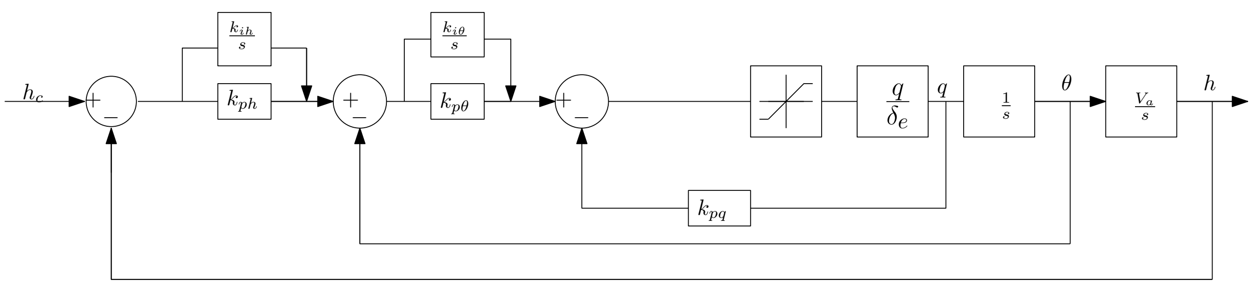

Fig. 7. Longitudinal controller structure

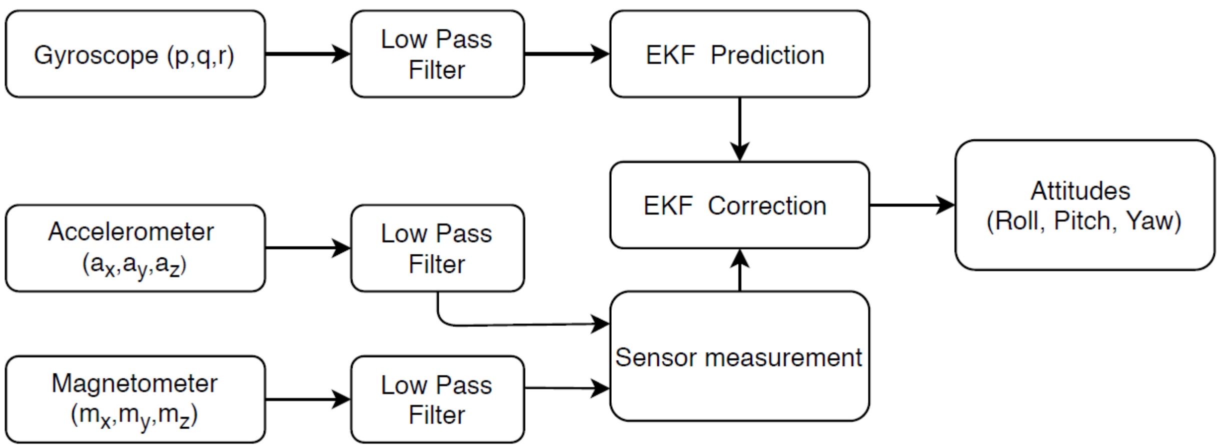

Fig. 8. Estimation block

Fig. 9. Motion simulator

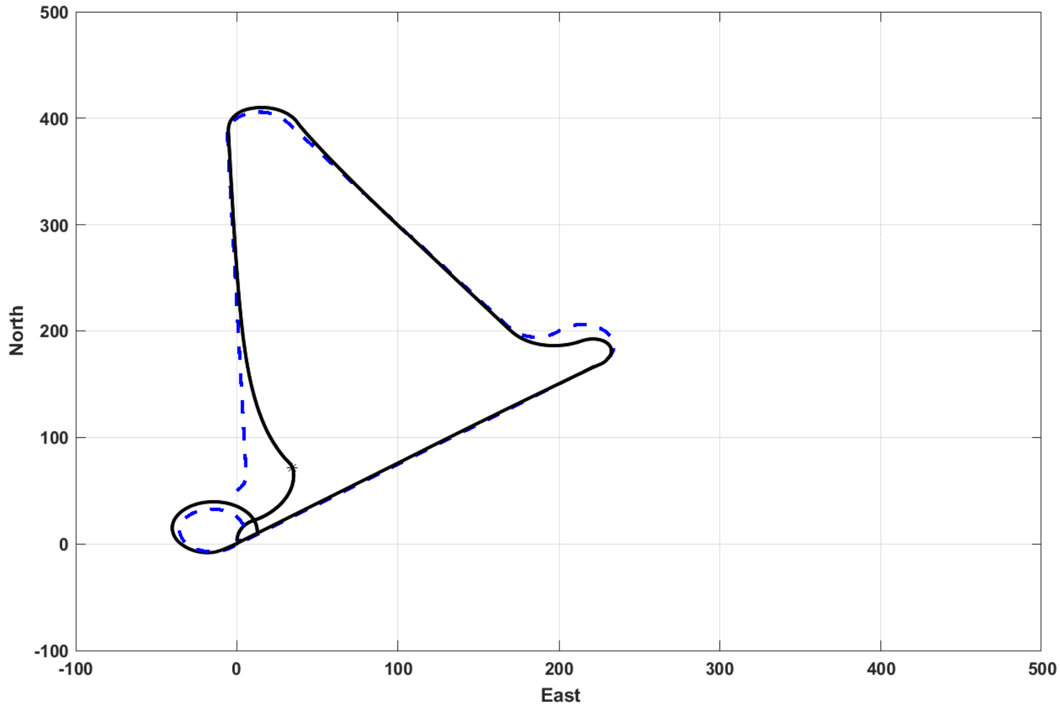

Fig. 10. Waypoint following (simulation): Solid line-Actual path, Dashed line-Desired path

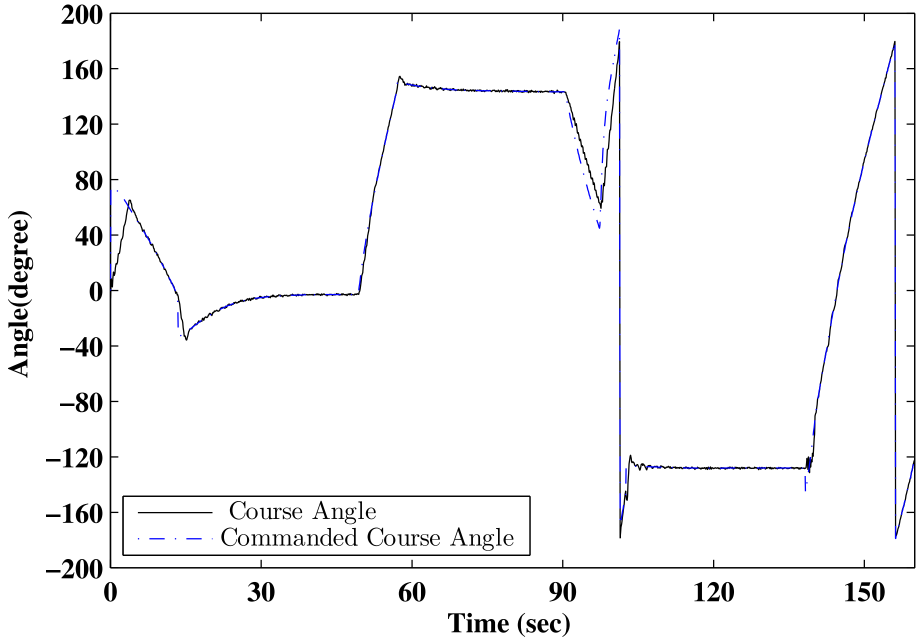

Fig. 11. Tracking of desired course angle

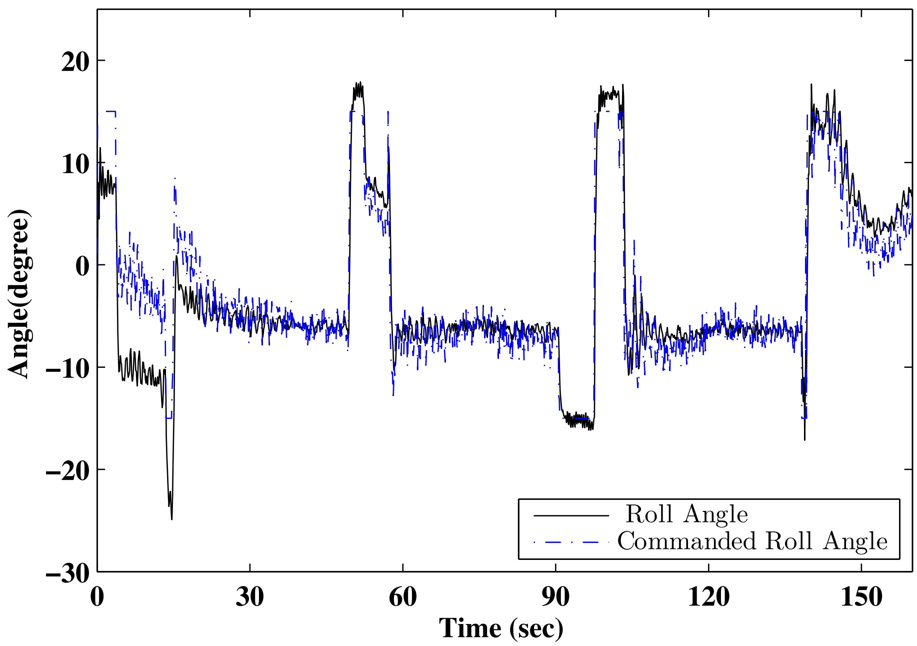

Fig. 12. Tracking of desired roll angle

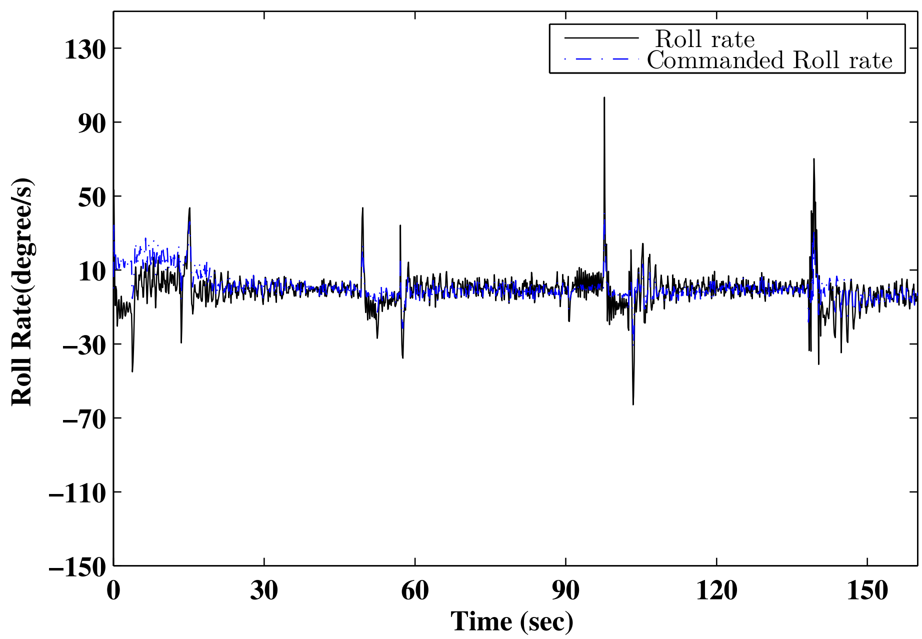

Fig. 13. Tracking of desired roll rate

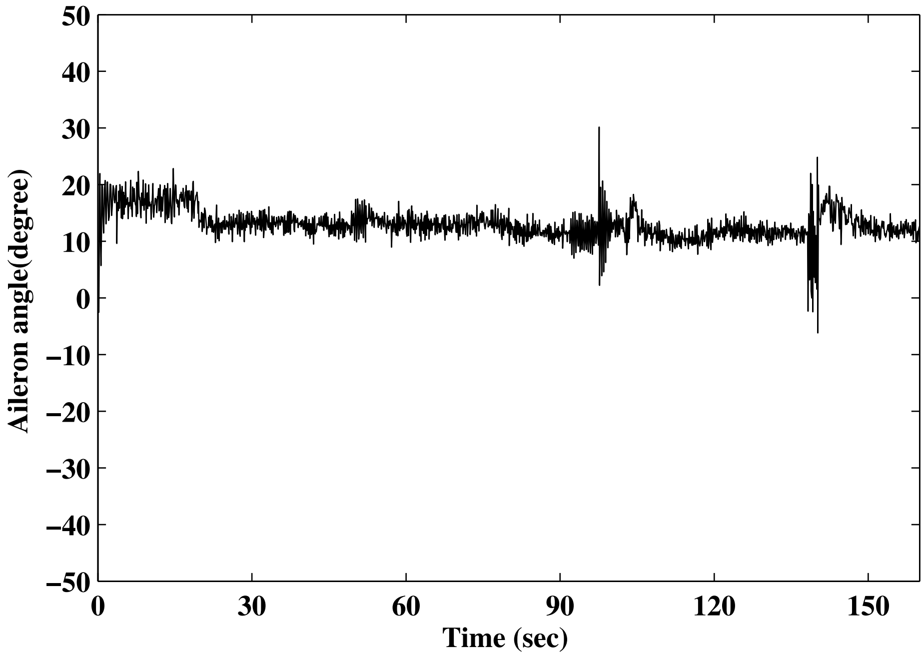

Fig. 14. Aileron Command

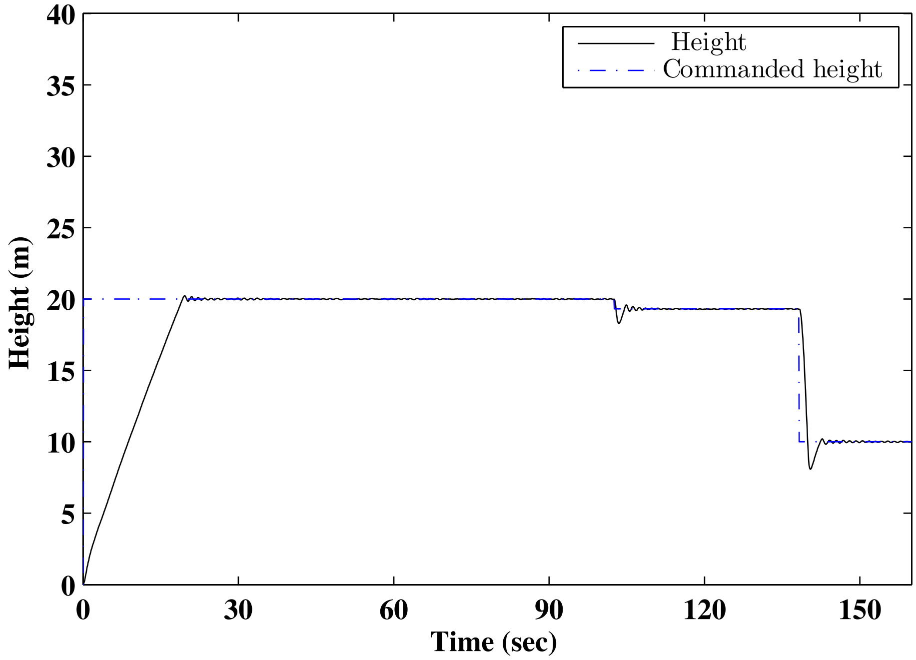

Fig. 15. Tracking of desired height

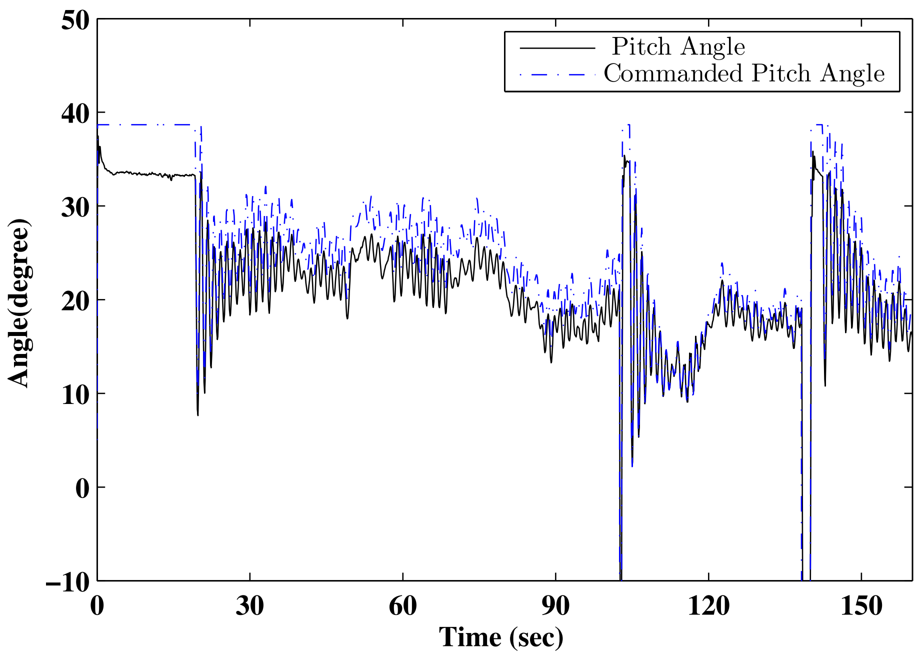

Fig. 16. Tracking of desired pitch angle

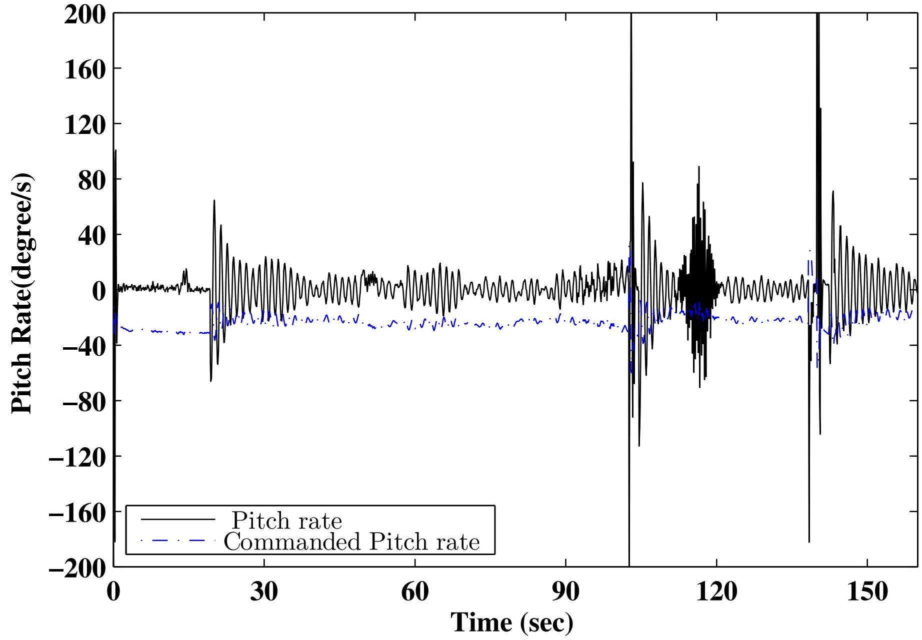

Fig. 17. Tracking of desired pitch rate

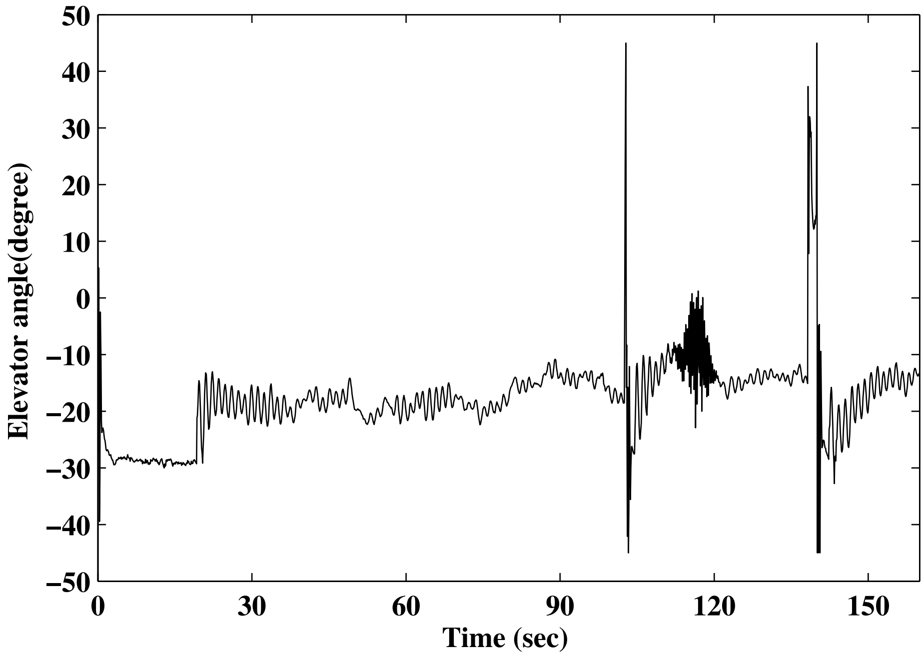

Fig. 18. Elevator Command

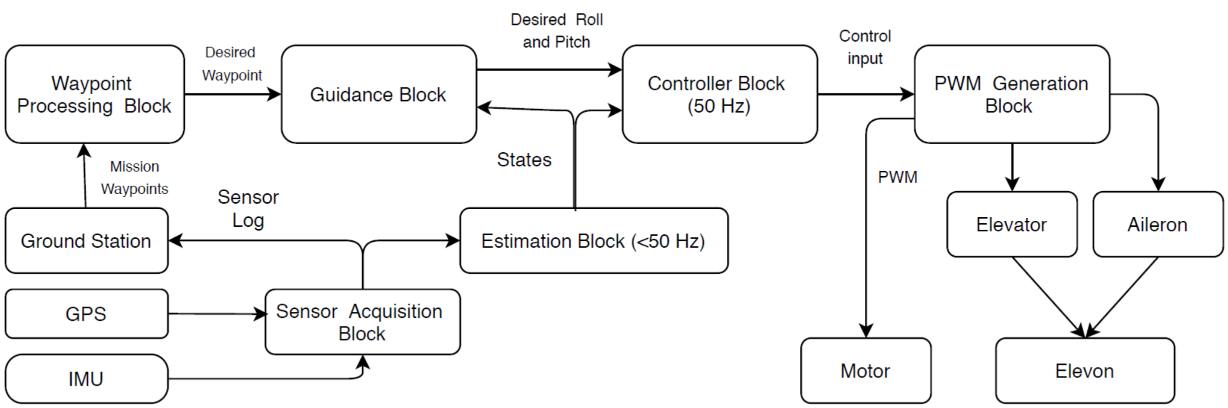

Fig. 19. Flow diagram for waypoint mission implementation

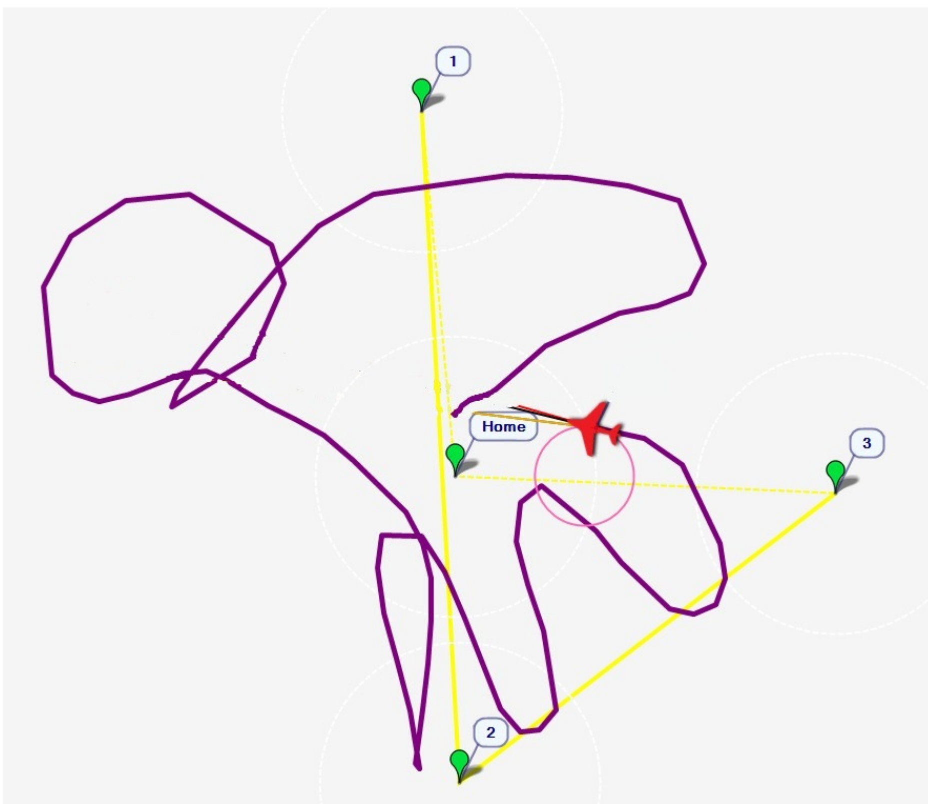

Fig. 20. Tracking of waypoint

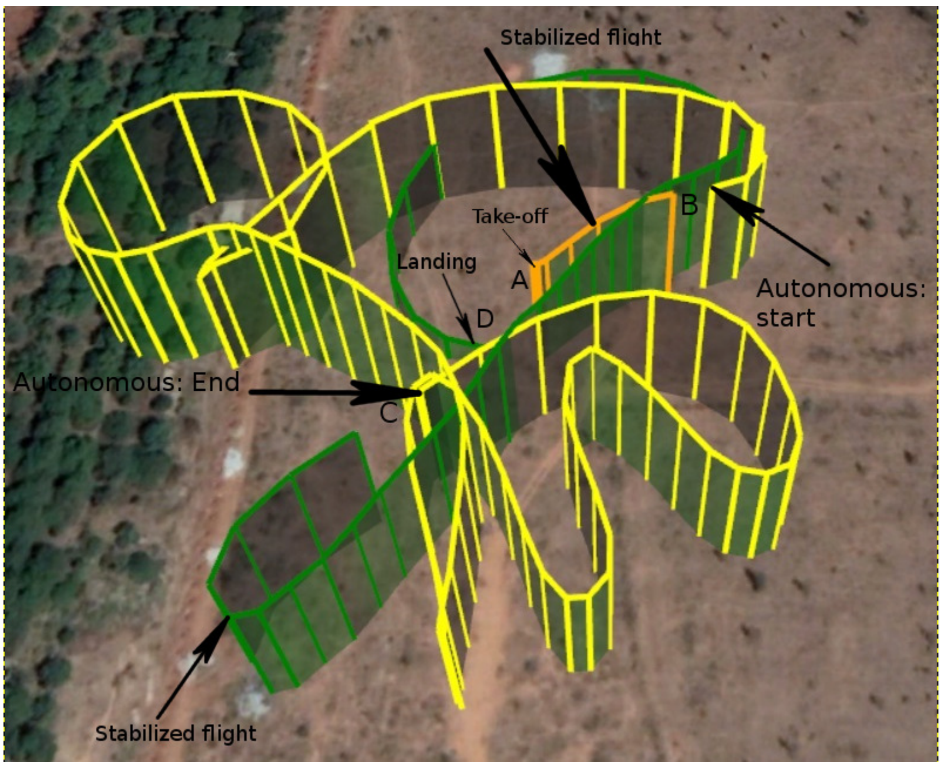

Fig. 21. 3D path during waypoint following

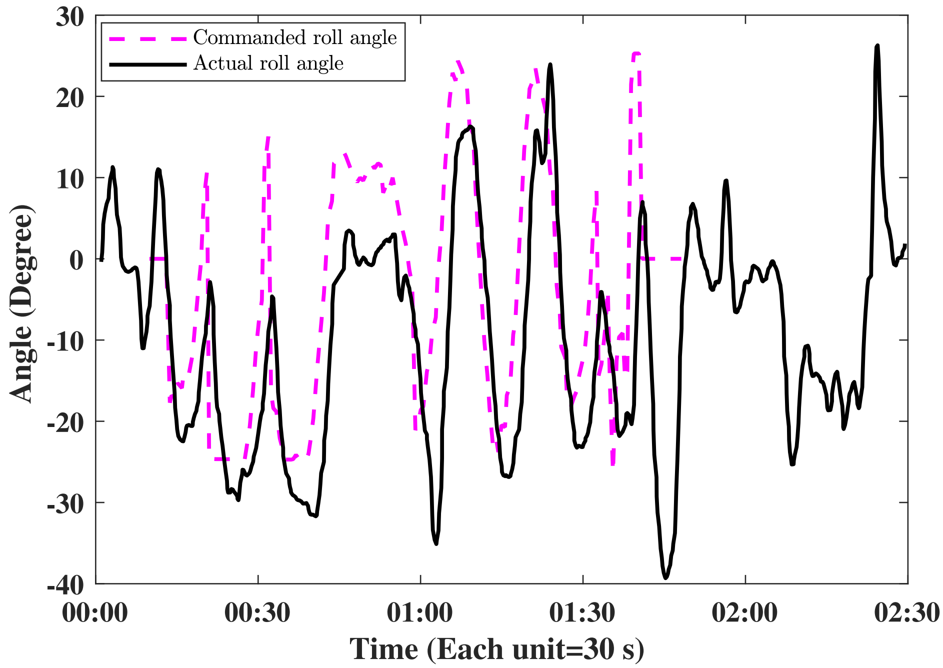

Fig. 22. Commanded roll angle vs Actual roll angle

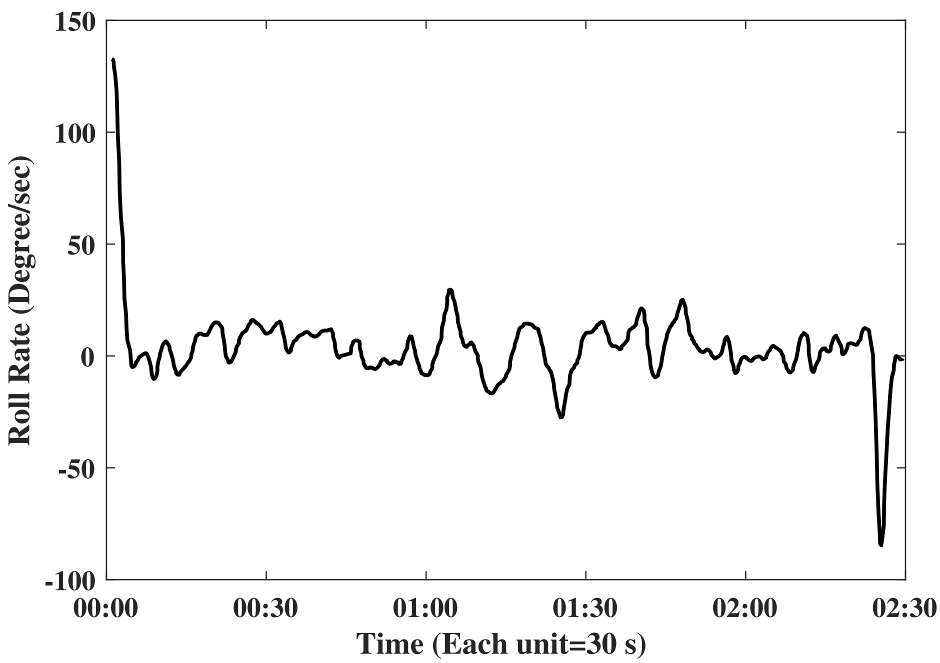

Fig. 23. Roll rate

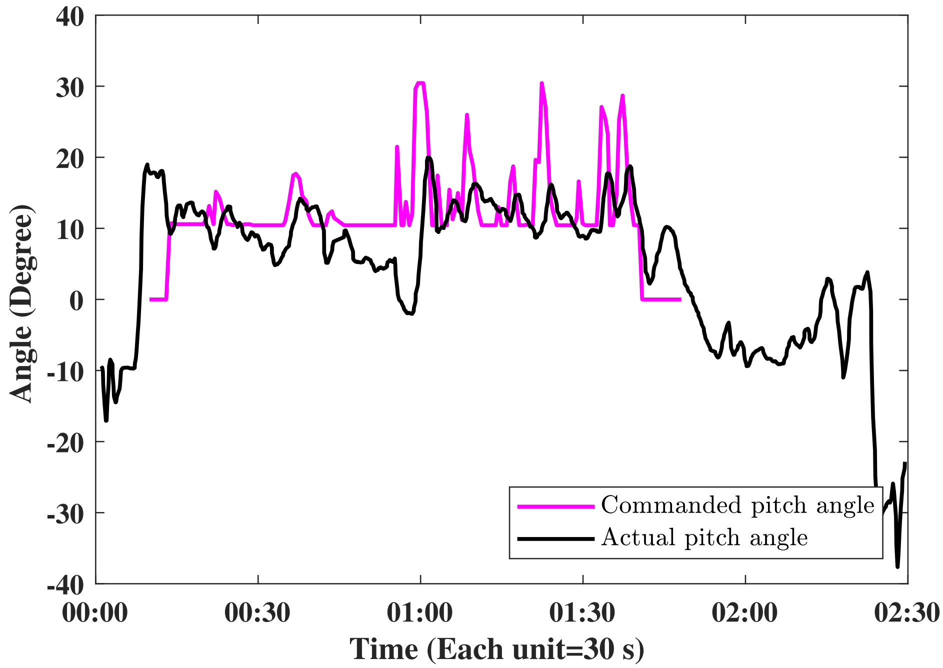

Fig. 24. Commanded pitch angle vs Actual pitch angle

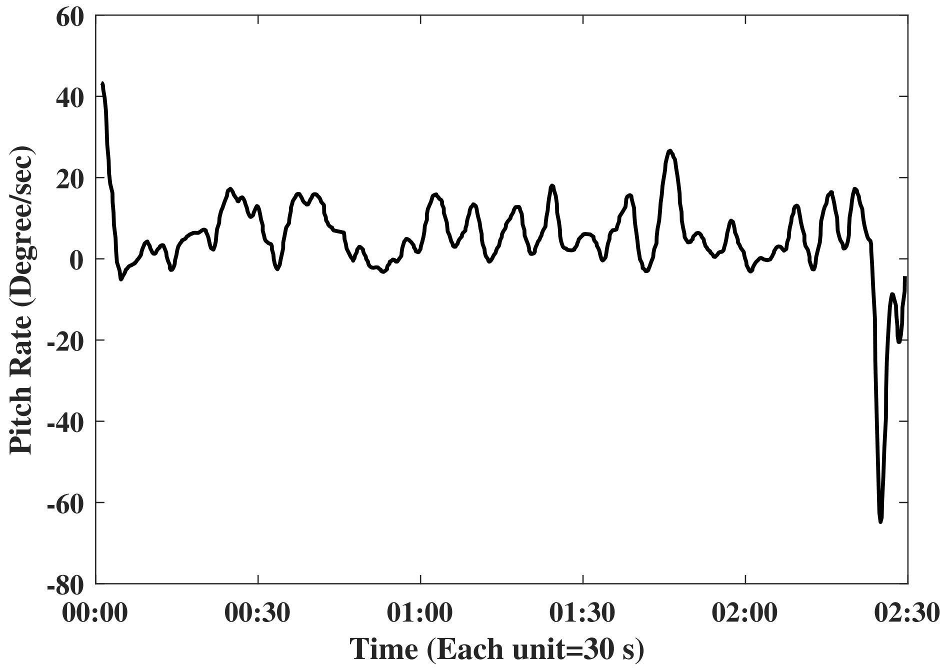

Fig. 25. Pitch rate

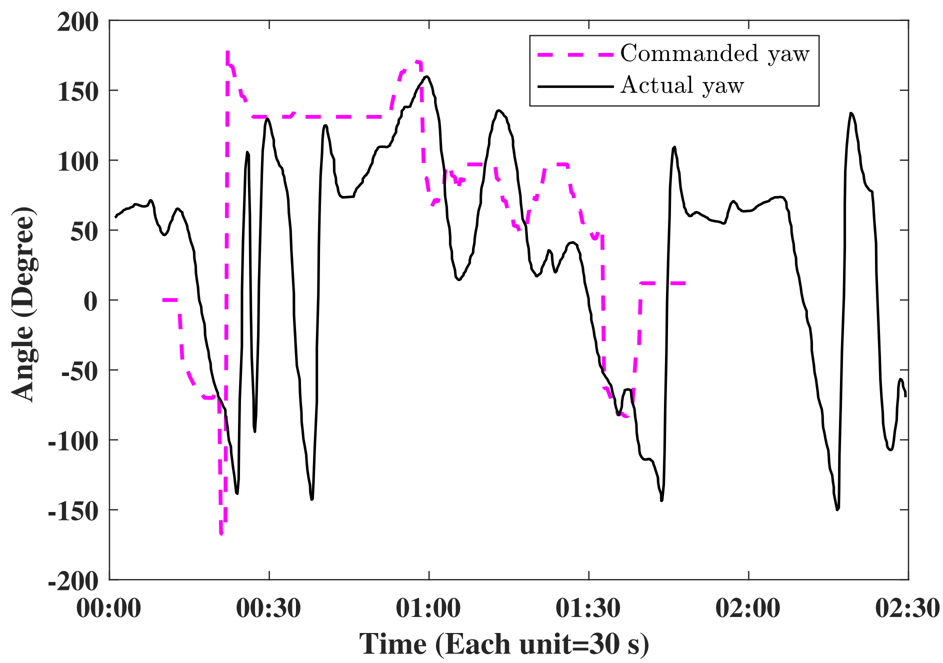

Fig. 26. Commanded yaw angle vs Actual yaw angle

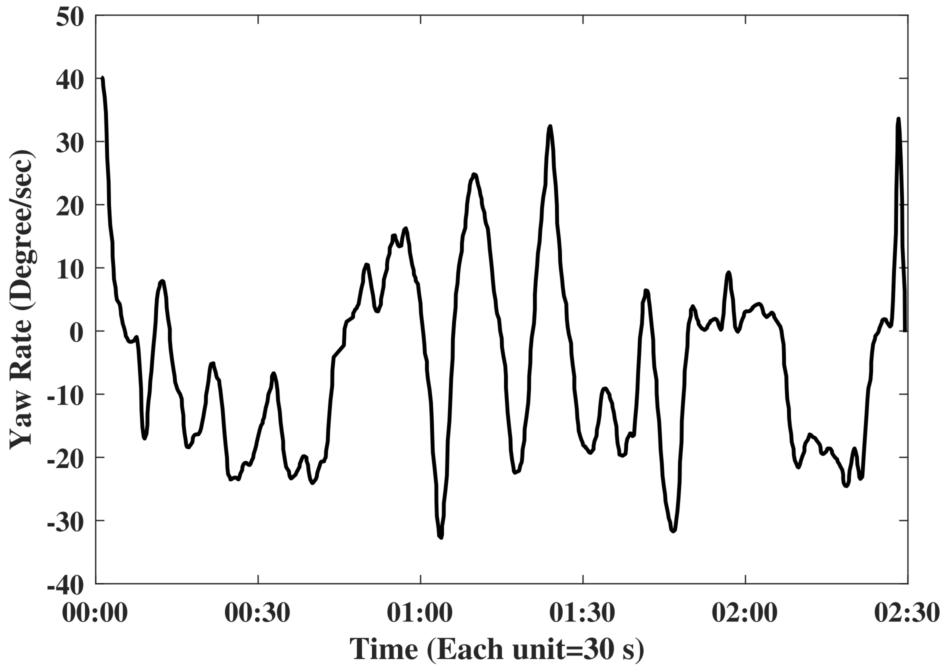

Fig. 27. Yaw rate